



HAL
open science

The resolvin D2 – GPR18 axis is expressed in human coronary atherosclerosis and transduces atheroprotection in apolipoprotein E deficient mice

Matthieu Bardin, Sven-Christian Pawelzik, Jeremy Lagrange, Ali Mahdi, Hildur Arnardottir, Véronique Regnault, Bruno Fève, Patrick Lacolley, Jean-Baptiste Michel, Nathalie Mercier, et al.

► To cite this version:

Matthieu Bardin, Sven-Christian Pawelzik, Jeremy Lagrange, Ali Mahdi, Hildur Arnardottir, et al.. The resolvin D2 – GPR18 axis is expressed in human coronary atherosclerosis and transduces atheroprotection in apolipoprotein E deficient mice. *Biochemical Pharmacology*, 2022, 201 (11), pp.115075. 10.1016/j.bcp.2022.115075 . hal-04020850

HAL Id: hal-04020850

<https://hal.science/hal-04020850>

Submitted on 9 Mar 2023

HAL is a multi-disciplinary open access archive for the deposit and dissemination of scientific research documents, whether they are published or not. The documents may come from teaching and research institutions in France or abroad, or from public or private research centers.

L'archive ouverte pluridisciplinaire **HAL**, est destinée au dépôt et à la diffusion de documents scientifiques de niveau recherche, publiés ou non, émanant des établissements d'enseignement et de recherche français ou étrangers, des laboratoires publics ou privés.



The resolvin D2 – GPR18 axis is expressed in human coronary atherosclerosis and transduces atheroprotection in apolipoprotein E deficient mice

Matthieu Bardin^a, Sven-Christian Pawelzik^{c,1}, Jeremy Lagrange^{a,b,1}, Ali Mahdi^c, Hildur Arnardottir^c, Véronique Regnault^a, Bruno Fève^d, Patrick Lacolley^a, Jean-Baptiste Michel^a, Nathalie Mercier^a, Magnus Bäck^{a,c,*}

^a Université de Lorraine, Inserm, DCAC, Nancy, France

^b CHRU Nancy, Vandœuvre-lès-Nancy, France

^c Department of Medicine Solna, Karolinska Institutet and Department of Cardiology, Karolinska University Hospital, Stockholm, Sweden

^d INSERM UMR_S938, Centre de recherche Saint-Antoine, Institut Hospitalo-Universitaire, Université de la Sorbonne, ICAN, 75012 Paris, France

ARTICLE INFO

Keywords:

Coronary artery disease
Inflammation
Macrophage
Specialized pro-resolving mediators

ABSTRACT

Chronic inflammation in atherosclerosis reflects a failure in the resolution of inflammation. Pro-resolving lipid mediators derived from omega-3 fatty acids reduce the development of atherosclerosis in murine models. The aim of the present study was to decipher the role of the specialized proresolving mediator (SPM) resolvin D2 (RvD2) in atherosclerosis and its signaling through the G-protein coupled receptor (GPR) 18. The ligand and receptor were detected in human coronary arteries in relation to the presence of atherosclerotic lesions and its cellular components. Importantly, RvD2 levels were significantly higher in atherosclerotic compared with healthy human coronary arteries. Furthermore, apolipoprotein E (ApoE) deficient hyperlipidemic mice were treated with either RvD2 or vehicle in the absence and presence of the GPR18 antagonist O-1918. RvD2 significantly reduced atherosclerosis, necrotic core area, and pro-inflammatory macrophage marker expression. RvD2 in addition enhanced macrophage phagocytosis. The beneficial effects of RvD2 were not observed in the presence of O-1918. Taken together, these results provide evidence of atheroprotective pro-resolving signalling through the RvD2-GPR18 axis.

1. Introduction

Atherosclerosis is in addition to elevated cholesterol-rich lipoproteins closely linked to chronic inflammation [1]. The immune responses of atherosclerosis include for example recruitment and activation of leukocytes, macrophage polarization, and synthesis of pro-inflammatory cytokines [2]. Advanced atherosclerotic lesions are characterized by the presence of a necrotic core, reflecting a malfunctioning efferocytosis and leading to insufficient clearance of apoptotic cells [3]. Taken together, the atherosclerotic lesion immune characteristics are concordant with a failure in the resolution of inflammation [4].

Resolution of inflammation is an active process to limit inflammatory activation to bring back the vascular wall to a homeostasis state. This protective mechanism can be mediated by for example lipid specialized

pro-resolving lipid mediators (SPM) [5], which signal through specific G protein-coupled receptors (GPR) [6]. In the context of atherosclerosis, exogenous administration of SPM has been consistently shown to reduce atherosclerosis in murine models [7–9]. Genetic modulation of SPM receptor expression in murine atherosclerosis has however generated contradictory results, indicating both beneficial effects [10,11] and exacerbated disease [12,13] transduced through these receptors. The latter observations reflect the importance of the balance between pro-inflammatory and pro-resolving ligands for the SPM receptors to determine the downstream signalling [7,14,15].

Among SPM, D-series resolvins, synthesized from the omega-3 polyunsaturated fatty acid (n-3 PUFA) docosahexaenoic acid (DHA), display protective effects against atherosclerosis progression, [8,11] which has also been demonstrated for their receptors ALX/FPR2 [7] and

* Corresponding author at: Department of Medicine, Karolinska Institutet, Department of Cardiology, Karolinska University Hospital, 14186 Stockholm, Sweden.
E-mail address: Magnus.Back@ki.se (M. Bäck).

¹ Equal contribution.

GPR32 [11]. Resolvin D2 (RvD2) promotes macrophage polarization towards a reparative phenotype, leading to plaque stabilization [8]. GPR18 was identified as receptor for RvD2 [16]. This receptor belongs to the orphan class A family and was identified as part of the endocannabinoid system, which plays a major role in energy homeostasis (modulation of caloric intake, nutrient transport, cellular metabolism, and energy storage) [17]. How the specific pathway involving RvD2 and GPR18 is affecting atherosclerosis has not been previously investigated.

The aim of this study was to decipher the implication of the RvD2-GPR18 axis in atherosclerosis. We explored the ligand and receptor in human coronary arteries in relation to the presence of atherosclerotic lesions and its cellular components. We furthermore treated hyperlipidemic mice with RvD2 with and without the GPR18 antagonist O-1918, to establish RvD2-induced effects through GPR18 on atherosclerotic plaque development, pro-inflammatory responses, and phagocytic activity. The study identified GPR18 and its ligand RvD2 in human coronary atherosclerosis and showed that this RvD2 reduced murine atherosclerosis. The effects of RvD2 were not observed in the presence of O-1918, indicating atheroprotective pro-resolving signalling through the RvD2-GPR18 axis.

2. Material and methods

2.1. Human tissues

Human coronary artery walls, including healthy and diseased arteries at different stages of atherosclerotic diseases, were collected from the Inserm human CV biobank (BB-0033-00029, U 1148, X. Bichat Hospital, Paris), included in the European network BBMRI-ERIC, in accordance with the French regular and ethical rules (BioMedicine Agency convention DC2018-3141) and the principles of the declaration of Helsinki. Approval was obtained from the French Biomedical Agency (ABM, PFS09-007 & PFS17-002) and the Institutional Ethical Review board (SC09-09-66). Tissues were obtained from deceased organ donors for kidney and/or hepatic transplantation in the absence of therapeutic uses for the heart. When collected, healthy coronary arteries were macroscopically analysed by a trained vascular surgeon (J-BM) to ensure that these samples were not pathological (absence of fatty streak or atherosclerosis plaques after longitudinal opening). For immunohistochemistry, human arterial tissues were fixed with 4% (w/v) buffered formaldehyde solution prepared by depolymerisation of paraformaldehyde and imbedded in paraffin. Serial 5 µm thick sections were collected.

Conditioned media were prepared from small pieces (about 2 mm³) of tissue, weighed, and incubated for 24 h in serum-free RPMI culture medium containing 1% L-glutamine, 1% penicillin, streptomycin, and amphotericin at 37°C (5% CO₂). For standardization, the volume of medium was adjusted to sample wet weight (6 mL per gram of tissue). Conditioned media were collected, centrifuged (14000g for 15 min at 4°C), and stored at -80°C until further analysis as previously described [18]. RvD2 concentrations in conditioned media were measured by ELISA (Cayman Chemical, Ann Arbor, USA, item 501120).

2.2. Animals

ApoE^{+/+} mice on a C57BL/6J background were obtained from Charles River (Wilmington, USA) and fed a standard diet. For the experimental protocols, 8–9 weeks old ApoE^{-/-} mice on a C57BL/6J background from Taconic Biosciences (Rensselaer, USA) were used. Housing and experiments were conducted in accordance with the French regulations and the experimental guidelines of the European Community (Directive 2010/63/EU). Animals were housed under standard conditions (22°C, day-night cycle of 12 h, 70% humidity) and given free access to high fat diet (HFD) containing 1.25% cholesterol (E15749-347; Ssniff, Soest, Germany). The protocols were approved by the Animal Ethics Committee of Lorraine, France (#9411-2017032718404787 v4).

Mice were fed HFD for 4 weeks and injected 3 times per week (IP, 100 µL) with the following: (1) vehicle consisting of saline solution and EtOH 2.8% (control group), (2) RvD2 (100 ng per mouse in 2.8% EtOH) (from Cayman Chemical, Ann Arbor, USA), (3) O-1918 in 2.8% EtOH (2 mg/kg) (from Tocris, Bristol, UK) or (4) a combination of RvD2 and O-1918. Mice were put to death after isoflurane anaesthesia (1.5% in 1 L/min oxygen) followed by cervical dislocation. Blood, heart, aorta, and peritoneal macrophages were collected for the experiments detailed below.

2.3. Measurements of plasma lipid and RvD2 levels

Triglyceride levels were measured using a glucose meter (Accutrend® Plus mmol/L), capable to measure triglycerides using specialized strips. Cholesterol levels were measured in mice plasma using ELISA assay (MyBiosource, San Diego, USA, item MBS269999). RvD2 concentrations in murine plasma samples were measured by ELISA (Cayman Chemical, Ann Arbor, USA, item 501120).

2.4. Evaluation of atherosclerotic lesions

Atherosclerotic lesion burden in the aortic arch and the thoracic aortas was determined by *en face* analysis. Dissected aortic arches were fixed in 4% PFA, cut longitudinally, and stained with Oil Red-O solution (Sigma-Aldrich, Saint-Louis, USA). Images were acquired using a light microscope (Nikon Eclipse Ci). Total area of the thoracic aorta and area of the atherosclerotic lesions, respectively, were quantified using ImageJ (NIH) to express the relative lesion area as percentage of the thoracic aorta area. Aortic roots were embedded in OCT (Leica, Wetzlar, Germany) and frozen at -80°C. Serial, 10 µm thick cryosections were collected, starting from the appearance of the aortic valve cusps, and fixed either with 4% PFA or acetone. PFA fixed section, collected every 100 µm from the aortic valve cusps, were stained with Oil Red-O (Sigma-Aldrich, Saint-Louis, USA). Images were acquired with a light microscope equipped with a DC300 camera (Leica, Wetzlar, Germany).

The area of the aortic root lesions was determined in a blinded fashion using ImageJ (NIH) and expressed relative to the total aortic root area. The area of necrotic cores, defined as unstained zones devoid of cells or extracellular matrix, was measured in a blinded fashion using ImageJ (NIH). In both cases, *i.e.* relative aortic root lesion area and relative necrotic core area, exclusion criteria were decided as follows: if two or more sections were missing between 200 and 600 µm past the aortic valve cusps, mice were excluded; if one section was missing, the value was imputed by the mean of the previous and the following value.

2.5. Immunohistochemistry

Human coronary artery histological sections were stained with anti-GPR18 antibody (Bioss Antibodies, Boston, USA; 1:100 dilution), anti-CD68 antibody (Abcam, Cambridge UK; 1:8000 dilution). Murine atherosclerotic lesion composition was analysed using immunohistochemistry in level-matched sections with anti-CD68 antibody (Serotec, UK; 1:20000), anti-iNOS antibody (Abcam, Cambridge, UK; 1:100), anti-Arginase-1 antibody (Abcam, Cambridge, UK; 1:50), and anti-CD206 antibody (Serotec, UK; 1:50) or an isotype control (Serotec, UK; 1:100) and secondary antibodies (Vector Labs, Newark, USA; 1:200) using a standard avidin-biotin-peroxidase complex method. 3,3'-diaminobenzidine (Vector Labs, Newark, USA) was then used as the substrate to localize the primary antibodies. The preparations were counterstained with haematoxylin, mounted with Permount (Merck, Darmstadt, Germany) and examined by light microscopy.

2.6. Quantitative real-time PCR

Total RNA was isolated from the abdominal aorta using QIAzol (Qiagen, Hilden, Germany) and Qiagen RNeasy Mini kit (Qiagen, Hilden, Germany). RNA concentrations were measured

spectrophotometrically using Nanodrop 1000 (Thermo Fisher Scientific, Waltham, USA), and reverse transcription was performed using the High-capacity RNA-to-cDNA kit (Thermo Fischer Scientific, Waltham USA). Quantitative real-time PCR was performed on a 7900HT Fast Real-Time PCR system (Thermo Fisher Scientific, Waltham, USA) with the following TaqMan Assay-on-Demand probes (Thermo Fisher Scientific, Waltham USA): iNOS (Mm00440502_m1), CD68 (Mm03047343_m1), CD206 (Mm01329359_m1), and Arg-1 (Mm00475988_m1) were used to evaluate expression, and HPRT (Mm03024075_m1) was used as housekeeping gene. Results are expressed as % of the control using the Δ Ct method.

2.7. Phagocytosis assay

Mice were intraperitoneally washed by injecting 5 mL PBS to obtain peritoneal macrophages. Cells were then plated in a black 96-well plate with clear bottom at 10^5 cells per well. After 24 to 48 hrs, cells were treated with FITC-labelled zymosan particles (Invitrogen, Carlsbad, USA) (10^6 particles per 10^5 cells) for 45 min before they were washed with PBS. The cells were then fixed with 4% PFA for 15 min, the nuclei were stained with DAPI, and the cells were observed under a fluorescence microscope. Quantification of fluorescence and nuclei count were performed with ImageJ software. Data are presented as fluorescence intensity plotted against the number of cells.

2.8. Erythrocyte isolation and incubation for ROS measurements

Whole blood was collected from the carotid artery into citrated tubes and centrifuged. The erythrocytes pellet was washed 3 times with PBS^{-/-} (followed each time by centrifugation at 1000g, 10 min, 4 °C) and incubated with the spin probe 1-hydroxy-3-methoxycarbonyl-2,2,5,5-tetramethylpyrrolidine (CMH) (200 μ M, Noxygen Science Transfer & Diagnostics GmbH, Elzach, Germany) to evaluate the production of reactive oxygen species. In brief, 5 μ L of washed erythrocytes were added to 1 mL CMH:KREBS/HEPES solution, (1:1, v/v), mixed well, and incubated for 30 min at 37 °C with gentle shaking. Incubations were stopped by freezing the samples on dry ice. Samples were stored at -80 °C until ROS production was quantified with electron paramagnetic resonance (EPR) using Bruker E-Scan M system (Bruker, Billerica, USA) as previously described [28] with the following settings: center field 1.99 g, microwave power 1 mW, modulation amplitude 9 G, sweep time 10 s, number of scans 10, field sweep 60 G. The EPR spectrums are expressed % of control.

2.9. Statistical analysis

Data are presented as mean \pm SEM. For comparison between two groups, non-normally distributed data were compared using a Mann-Whitney Rank Sum test, whereas normally distributed data were compared by a two-tailed either paired or unpaired Student *t* test. One-way ANOVA was performed when comparing multiple groups. For the aortic root lesions and necrotic core analysis, two-way ANOVA followed by Tukey's multiple comparison was performed, $p < 0.05$ was considered as statistically significant. Phagocytosis assay was analyzed using linear regression and comparison between the groups was performed by multivariable linear regression. Chi square test was used to evaluate differences between groups in human immunohistochemistry classification. Statistical analysis was performed using Graphpad prism 8.0.2 software. $p < 0.05$ was considered as statistically significant.

3. Results

3.1. Resolvin D2 and GPR18 in human coronary artery atherosclerosis.

Conditioned media was prepared from endarterectomies of $n = 7$ healthy coronary arteries (100% male, mean age 42 ± 18.7 years) and n

$= 23$ atherosclerotic coronary artery segments (100% male, mean age 59 ± 8.4 years). The concentrations of RvD2 were significantly higher in conditioned media derived from patients with atherosclerotic coronary arteries compared with healthy coronary arteries (Fig. 1A). GPR18 immunostaining was detected in 41 of 42 human coronary segments examined. Staining in consecutive sections indicated co-localization of GPR18 and CD68 immunoreactivity (Fig. 1B).

The immunostainings for GPR18 and CD68 were categorized into negative (light blue), low expression (blue), and moderate expression (dark blue) for $n = 42$ sections (74% males, mean age 57.6 ± 7.1 years) (Fig. 1C and D). The CD68 immunostainings trended to gradually increase during disease progression from healthy ($n = 14$, 57.1% males, mean age 56.6 ± 7.3 years) through fatty streaks ($n = 9$, 40% males, mean age 60.7 ± 8.8 years) to established atherosclerotic lesions ($n = 19$, 96.1% males, mean age 57.7 ± 5.9 years). In contrast, GPR18 exhibited in the same coronary segments a bell-shaped expression pattern with increased expression at early stages of atherosclerosis (fatty streaks) followed by decreased expression similar to controls in established atherosclerotic lesions (Fig. 1D).

3.2. Resolvin D2 decreased murine aortic root atherosclerosis through GPR18

Plasma levels of RvD2 were significantly lower in HFD-fed ApoE^{-/-} mice compared with chow-fed ApoE^{+/+} mice (105 ± 7.8 pg/mL; $n = 15$ vs. 533 ± 108 pg/mL; $n = 4$; $p < 0.05$). Quantification of atherosclerotic plaque burden in the aortic root are shown in Fig. 2A-B. ApoE^{-/-} mice were subjected to intraperitoneal injections with either RvD2 or O-1918 alone or in combination followed by quantification of atherosclerotic plaque burden in the aortic root (Fig. 2AB) and thoracic aorta (C). Separating groups of mice in the absence or presence of the GPR18 antagonist O-1918 revealed that RvD2 significantly decreased atherosclerosis compared to the control group (Fig. 2A, $p < 0.001$). In contrast, RvD2 in combination with O-1918 did not significantly alter the relative atherosclerotic lesion size compared with mice treated with O-1918 alone (Fig. 2B, $p = 0.42$). The *en face*-quantified atherosclerotic lesion burden in the aortic arch and thoracic aorta was low without significant differences between the groups (Fig. 2C). There was no significant difference between the groups for blood cell counts, red blood cells parameters (Table 1), cholesterol or triglycerides (Table 2).

3.3. Necrotic core area decreased following RvD2 treatment

Necrotic core areas were measured in the aortic root (Fig. 3). In mice treated with RvD2, necrotic core areas were significantly reduced compared to mice from the control group [$p = 0.011$] (Fig. 3A). In O-1918-treated mice, necrotic core areas were not significantly altered by the combination of O-1918 and RvD2 compared with O-1918 alone [$p = 0.59$] (Fig. 3B).

3.4. Plaque macrophage phenotypes

Since GPR18 expression was present in CD68 positive areas of human atherosclerotic lesions (Fig. 1B), macrophage markers were monitored in murine lesions. Aortic root sections positive for CD68 were stained for M2 macrophages markers and showed low expression of the M2 marker CD206 and a highly variable expression pattern for Arginase-1 (Arg-1). Staining for the M1 marker iNOS yielded a positivity of approximately 10% of the lesion area (Fig. 3C and D). To provide a quantification of the effects induced by the treatment on lesional macrophage subtypes, qPCR analysis was performed and revealed a significant decrease of aortic iNOS expression in the aortas of RvD2-treated compared with vehicle-treated mice (Fig. 3E). In mice treated with O-1918, aortic iNOS expression was not significantly altered by RvD2 (Fig. 3F). The qPCR analysis of aortic expression of CD68, CD206, and Arg-1 did not reveal any significant difference between the groups (data not shown).

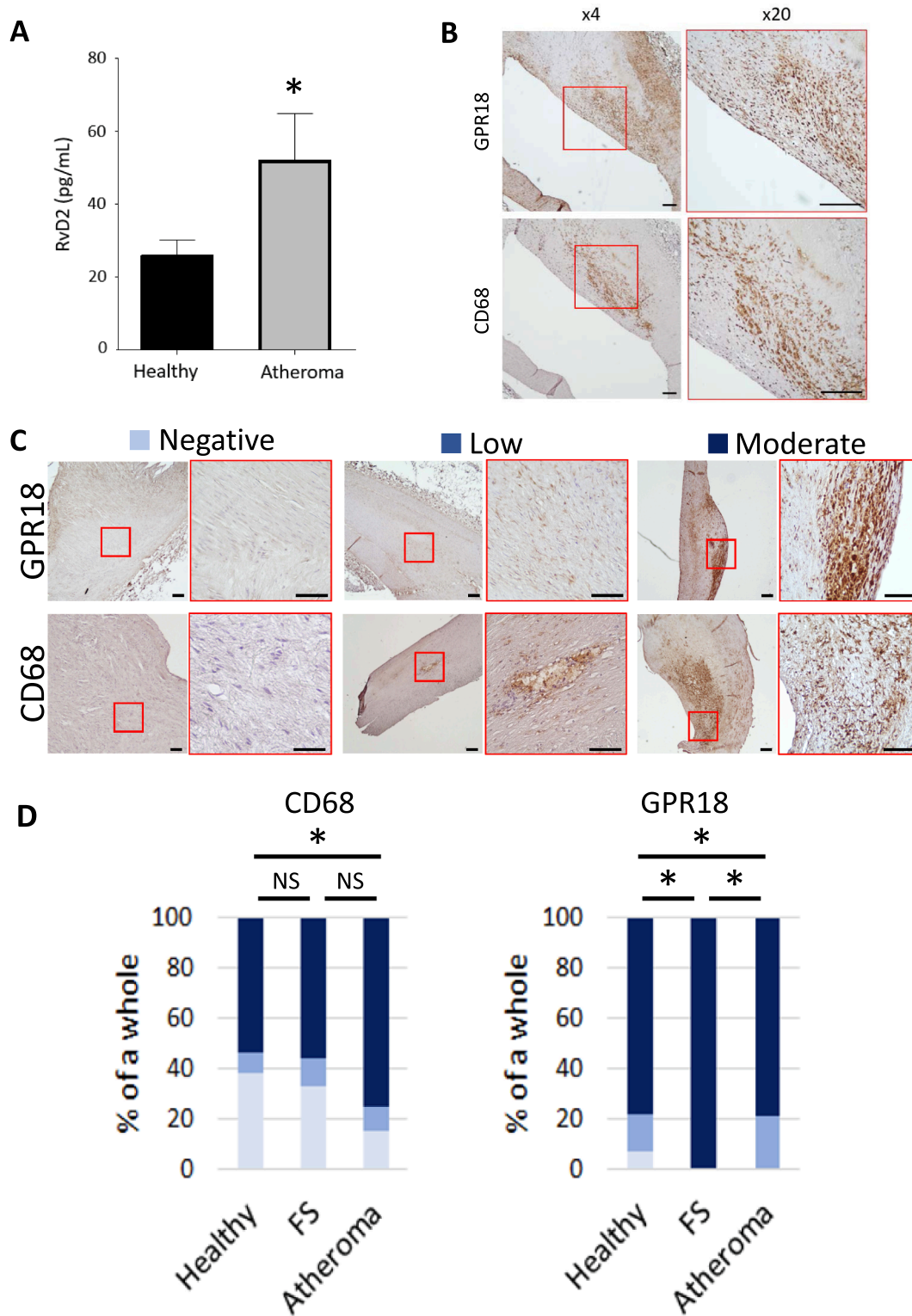


Fig. 1. Biosynthesis of resolvins D2 and expression of GPR18 receptor in human coronary arteries. A. Measurement of resolvins D2 (RvD2) in conditioned media prepared from human healthy and atherosclerotic coronary endarterectomies. n = 7 in the healthy group and n = 23 in the atheroma group. B. Representative micrographs from atheroma coronary artery patient immunostained for GPR18 and CD68. C. Representative micrographs of coronary arteries with different classification of GPR18 and CD68 expression. D. Proportion of expression of CD68 and GPR18, respectively, in healthy, fatty streaks (FS), and atheroma arteries. Scale bar = 100 μ m. n = 14 in the healthy group, n = 9 in the fatty streak group, and n = 19 in the atheroma group. Data are presented as mean \pm SEM. *p < 0.05, NS: not significant, differences in the RvD2 concentration were evaluated using a Mann-Whitney test, differences between groups in human immunohistochemistry classification were evaluated using Chi square test.

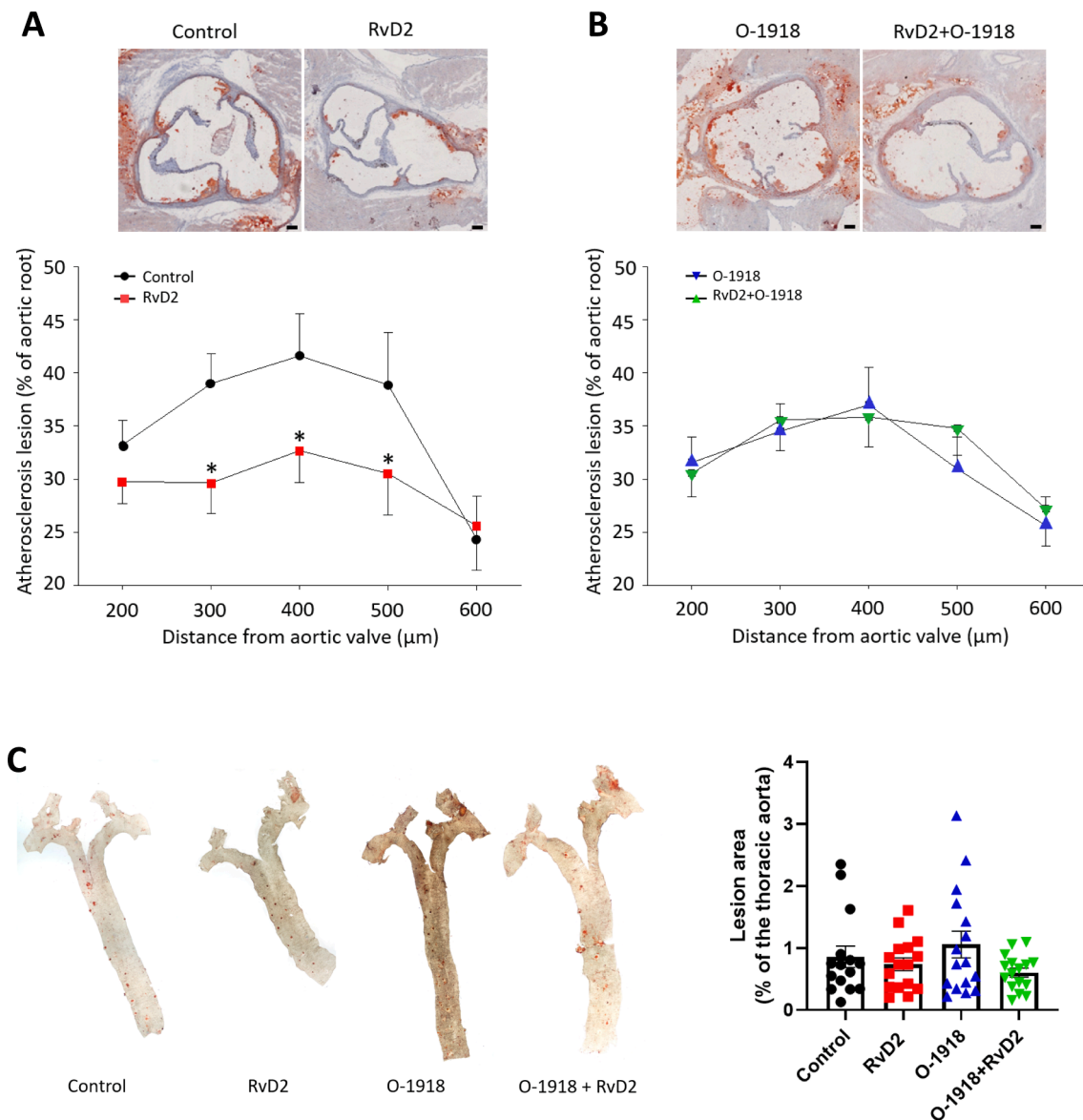


Fig. 2. Effect of RvD2 treatment on murine atherosclerosis development in the aortic root mediated through GPR18. **A.** Quantification of relative aortic root lesion size in ApoE^{-/-} mice treated with RvD2 vs control mice (n = 11–15 per group). *p < 0.05 vs Control (Two-way ANOVA followed by Tukey's multiple comparison) Representative images of aortic root sections stained with oil red O are shown above the graph Scale bar = 100 μm. **B.** Quantification of relative aortic root lesion size in ApoE^{-/-} mice treated with O-1918 vs O-1918 + RvD2 treated mice (n = 11–15 per group). (Two-way ANOVA: NS) Representative images of aortic root sections stained with oil red o are shown above the graph. Scale bar = 100 μm. **C.** Representative images of *en face*-stained thoracic aortas (left) and quantification of the relative plaque area (n = 15–16 per group). (One-way ANOVA: NS) Data are presented as mean ± SEM. (For interpretation of the references to colour in this figure legend, the reader is referred to the web version of this article.)

3.5. Macrophage phagocytosis and red blood cell-dependent ROS formation

The ability of macrophages for phagocytosis is central in inflammation resolution. Therefore, we isolated peritoneal macrophages from the four groups of mice and measured uptake of zymosan. Zymosan uptake was linearly related to the cell density. Representative images are shown in Fig. 4A. Because the cell numbers varied between experiments, the FITC fluorescence for all technical repeats (n = 6 per mouse) were plotted against the number of cells in each evaluated area. The linear regression for controls (n = 60 from n = 10 mice, adjusted $r^2 = 0.94$) had a slope of 0.51, whereas the linear regression for RvD2-treated mice (n = 60 from n = 10 mice, adjusted $r^2 = 0.80$) had a slope of 0.95 (Fig. 4B). Multiple linear regression determined that phagocytosis (p = 0.009) but not cell number (p = 0.16) significantly predicted the control *versus*

RvD2-treated groups from a linear combination of the independent variables. The treatment with a combination of RvD2 with O-1918 reverted regression to the control (slope: 0.55, adjusted $r^2 = 0.79$, n = 60 from n = 10 mice) (data not shown).

Uptake mechanisms in atherosclerosis also involve red blood cells. Their ability to release haemoglobin followed by haeme oxidation induces a pro-atherogenic oxidant stimulus. Red blood cell-dependent ROS formation measured by EPR indicated a significantly reduced ROS production by red blood cells derived from RvD2- compared with vehicle-treated mice. (Fig. 4C). In contrast, ROS production in mice treated with O1918 was similar in the absence and presence of RvD2 treatments (Fig. 4C), representative curves of ROS measurements are shown in Fig. 4C.

Table 1

Blood cell count from high fat diet-fed ApoE^{-/-} mice treated with vehicle (Control), RvD2, O-1918 or RvD2 + O-1918, respectively.

	Control	RvD2	O-1918	O-1918 + RvD2	p
White blood cells - 10 ³ /mm ³	5.46 ± 0.82	6.37 ± 1.58	5.48 ± 0.71	5.98 ± 1.36	0.94
Red blood cells - 10 ⁶ /mm ³	8.01 ± 0.15	7.72 ± 0.2	7.82 ± 0.19	8.04 ± 0.23	0.64
Hemoglobin - g/dl	11.7 ± 0.22	11.5 ± 0.21	11.5 ± 0.26	11.7 ± 0.33	0.87
Hematocrit - %	36.6 ± 0.72	36.2 ± 0.71	35.5 ± 0.8	36.9 ± 1.1	0.86
Platelet - 10 ³ /mm ³	525 ± 38.97	544 ± 24.1	500 ± 39.1	494 ± 32.86	0.73
MCV - μm ³	45.8 ± 0.14	46.8 ± 0.58	46.1 ± 0.2	46.0 ± 0.16	0.13
MCHC - g/dl	32.0 ± 0.15	31.9 ± 0.14	32.0 ± 0.08	31.8 ± 0.12	0.67
MPV - μm ³	6.45 ± 0.6	5.62 ± 0.25	5.38 ± 0.32	5.30 ± 0.21	0.15
Lymphocytes - 10 ³ /mm ³	3.63 ± 0.36	3.66 ± 0.34	4.13 ± 0.55	4.76 ± 1.19	0.68
Monocytes - 10 ³ /mm ³	0.31 ± 0.07	0.25 ± 0.05	0.36 ± 0.08	0.33 ± 0.09	0.81
Granulocytes - 10 ³ /mm ³	0.98 ± 0.17	0.76 ± 0.09	0.84 ± 0.09	0.89 ± 0.12	0.70

Results are expressed as mean ± SEM. MCV, mean corpuscular volume; MCHC, mean corpuscular hemoglobin concentration; MPC, mean platelet volume.

Table 2

Cholesterol and triglyceride blood levels from high fat diet-fed ApoE^{-/-} mice treated with vehicle (Control), RvD2, O-1918 or RvD2 + O-1918, respectively.

	Control	RvD2	O-1918	O-1918 + RvD2	p
Cholesterol (mmol/L)	151 ± 21.2	175 ± 35.6	122 ± 18.4	137 ± 28.6	0.55
Triglycerides (mmol/L)	1.92 ± 0.17	2.12 ± 0.23	1.98 ± 0.14	1.87 ± 0.18	0.77

Results are expressed as mean ± SEM.

4. Discussion

The results of the present study point to the RvD2-GPR18 axis transducing atheroprotective effects. First, the ligand and receptor were identified in human coronary atherosclerotic lesions. Second, RvD2 treatment of mice decreased atherosclerosis burden and necrotic core size. Third, decreased aortic iNOS expression and increased macrophage phagocytosis were observed in RvD2-treated mice. Fourth, the RvD2-induced effects were not observed in the presence of the GPR18 antagonist O-1918. Taken together, these results suggest GPR18 activation by RvD2 as a possible driver of beneficial actions through an inflammation resolution in atherosclerosis development.

SPM may play a key role in inflammation resolution and in cardiovascular disease progression. The balance between pro-inflammatory and pro-resolving lipid mediators is of particular relevance since previous studies have identified a decreased SPM to leukotriene ratio in human vulnerable atherosclerotic lesions [14] and in association with subclinical atherosclerosis [19]. This is the first report of RvD2 release from human atherosclerotic lesions in conditioned media prepared from human coronary arteries. Previous reports indeed confirmed the ability of human atherosclerotic lesion to metabolize DHA into D-series resolvins, although RvD2 was undetectable from carotid arteries [14]. In the present study, an increased RvD2 release was observed from coronary arteries affected by atheroma. These findings are in contrast to the decreased levels of RvD2 with progression of murine atherosclerosis [8], which was confirmed in the present study.

Even if the specificity of RvD2 measurements by ELISA compared

with LC-MS/MS identification, the low cross-reactivity with structurally similar lipid mediators (e.g. 17-HDHA and RvD1) taken together with the shared biological activities between RvD2 stereoisomers support that that measured changes in lipid mediators between groups are comparable between the two platforms [20]. An increased RvD2 synthesis in atherosclerotic lesions is further supported when interrogating the STARNET (Stockholm-Tartu Atherosclerosis Reverse Networks Engineering Task) containing data on increased expression of the RvD2 biosynthetic 5- and 15 lipoxygenases in human atherosclerotic aortic root samples compared with atherosclerosis-free internal mammary artery [21].

The next step in the regulation of pro-resolving effects is the expression of functional SPM receptors. We localized GPR18 expression in human atherosclerotic coronary arteries within CD68 positive areas, indicating macrophages as possible effectors of RvD2-induced effects. However, while the expression of CD68 was increasing with the coronary lesion progression, GPR18 exhibited an initial increase but decreased expression at more advanced stages. These results indicate that a functional RvD2 response towards a resolution of inflammation may be limited by a loss of GPR18 expression.

The notion of a beneficial role of RvD2 in atherosclerosis was raised by limitation of atheroprotection in mice treated with a combination of the two DHA metabolites RvD2 and maresin 1 [8]. However, the individual role of the two SPM and their receptors have not been previously investigated. Our results extend the findings by demonstrating that RvD2 treatment attenuated atherosclerosis. The GPR18 antagonist O-1918 exerted a tendency towards beneficial effects. O-1918 is however not a selective antagonist for GPR18 and has been reported to act also at GPR55 [22]. The decreased atherosclerosis by O-1918 in the present study may hence reflect effects on endocannabinoid signaling, which in addition to cannabinoid (CB) receptors can be transduced through GPR18 and GPR55. Importantly, RvD2 did not affect the atherosclerosis development in the presence of O-1918, pointing to RvD2 atheroprotective action being mediated by its ligation with GPR18.

Another complexity of the SPM ligand-receptor interaction is the presence of pro-inflammatory agonists for SPM receptors. For example, the RvD1 and LXA4 receptor ALX/FPR2 activated by formylated bacterial peptides and pro-inflammatory serum amyloid A (SAA) transduces a pro-atherogenic response reflected by atheroprotection in mice lacking the murine ALX/FPR2 homologue when SAA prevails [15] but blunted effects of exogenous LXA4 administration [7]. Likewise, deletion of the RvE1 receptor ERV1/ChemR23 has been reported to either reduce [13] or enhance [10] atherosclerosis progression, which may depend on agonist availability for receptor ligation.

In addition to smaller lesion size, the necrotic core area was reduced in mice treated with RvD2, whereas RvD2 was devoid of significant effects on the necrotic core in the presence of the GPR18 antagonist O-1918. This is in line with the increased necrotic core in ChemR23 deficient ApoE^{-/-} mice, [10], which may reflect the macrophage phenotypic change from pro-inflammatory towards pro-resolving subtypes [23,24] and increased phagocytic activity [10]. In line with the colocalization of GPR18 with macrophages in human plaques, we detected a decreased aortic iNOS expression in response to RvD2 in the absence but not in the presence of GPR18 antagonism, suggesting less pro-inflammatory macrophage phenotypes. RvD2 has previously been shown to facilitate macrophage differentiation towards pro-resolving phenotypes [25]. In addition, we found in macrophages isolated from the different groups of mice that RvD2 treatment resulted in an increased phagocytic activity which is a key mechanism of inflammation resolution and of importance to limit plaque development and enhance its stability [26]. The observation that RvD2 treatment did not alter cholesterol and triglyceride levels, which are of key importance in atherosclerosis development and progression, supports RvD2-induced atheroprotective effects that enhance macrophage phagocytosis.

Oxidative stress is another key mechanism in atherosclerosis development [27], in which erythrocytes play a major role [28]. When

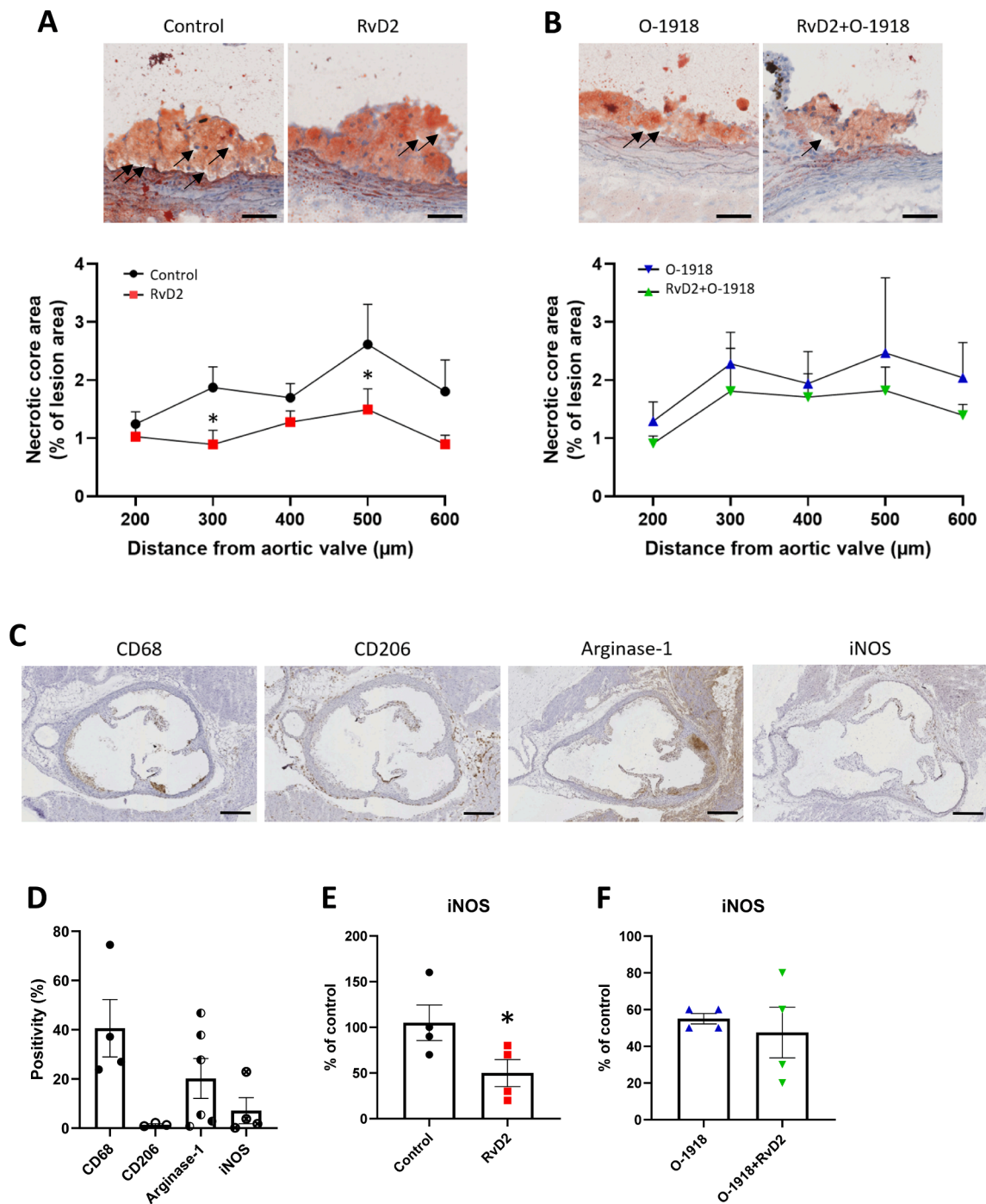


Fig. 3. Relative necrotic core area and histological characterization of atherosclerotic plaques following RvD2 treatment and GPR18 inhibition, respectively. **A.** Quantification of the relative necrotic core area in aortic root plaques from ApoE^{-/-} mice treated with RvD2 vs control mice (n = 11–14 per group). *p < 0.05 vs Control (Two-way ANOVA followed by Tukey's multiple comparison). Representative images are shown above the graph. Scale bar = 50 μm. Black arrows indicate necrotic areas. **B.** Quantification of the relative necrotic core area in aortic root plaques from ApoE^{-/-} mice treated with O-1918 vs O-1918 + RvD2 treated mice (n = 11–14 per group) (Two-way ANOVA: NS). Quantification of the relative necrotic core area in aortic root plaques from ApoE^{-/-} mice treated with O-1918 vs O-1918 + RvD2 treated mice (n = 11–14 per group). (Two-way ANOVA: NS). Representative micrographs of immunohistochemistry staining with Hematoxylin are shown. Scale bar = 50 μm. Black arrows indicate necrotic areas. **C.** Representative micrographs of immunohistochemistry staining in the aortic root stained for CD68, CD206, Arginase-1, and iNOS, respectively, scale bar = 250 μm. **D.** Quantification of immunohistochemistry staining intensity in aortic roots stained for CD68, CD206, Arginase-1, and iNOS. **E.** Comparison of iNOS mRNA expression in the abdominal aorta obtained from control and RvD2-treated ApoE^{-/-} mice (n = 4 per group). **F.** Comparison of iNOS mRNA expression in the abdominal aorta obtained from O-1918 and O-1918 + RvD2-treated ApoE^{-/-} mice. Data are presented as mean ± SEM. Differences between two groups were evaluated using an unpaired student t test, *p < 0.05. (For interpretation of the references to colour in this figure legend, the reader is referred to the web version of this article.)

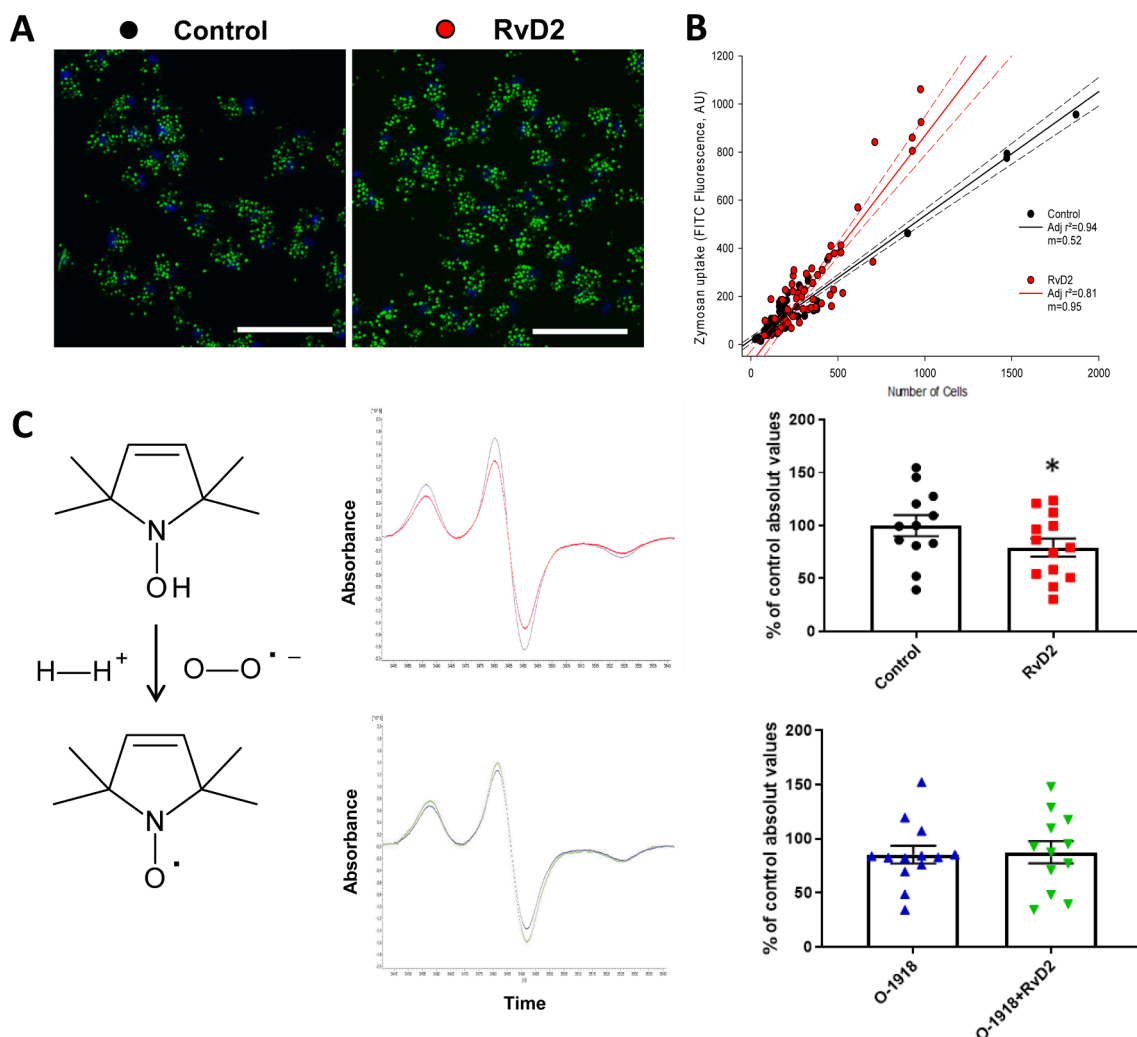


Fig. 4. Macrophage phagocytosis and red-blood cell-dependent formation of reactive oxygen species. **A.** Representative images of peritoneal macrophages from ApoE^{-/-} mice incubated with zymosan-FITC particles. Scale bar = 100 μ m. **B.** Quantification of phagocytosis expressed as zymosan uptake per number of macrophages. (n = 10 per group). **C.** Illustration showing oxidation of CMH-hydrochloride probe by ROS into EPR visible species (left). Representative curves obtained by EPR spectroscopy from the measurement of ROS produced by red blood cells (middle) and measurement of ROS production by red blood cell following CMH-hydrochloride incubation (right) (n = 11–12 per group). *p < 0.05 vs Control (paired student *t* test). (For interpretation of the references to colour in this figure legend, the reader is referred to the web version of this article.)

phagocytized by vascular smooth muscle cells, the internalization of erythrocytes is responsible for a strong oxidative stress [29]. The use of EPR to investigate the RvD2-GPR18 axis on ROS production indicated a significant decrease in ROS production by erythrocytes in mice treated with RvD2 compared to control mice.

Since RvD2 and/or O-1918 treatments did not affect plaque size in the thoracic aorta while more advanced lesions in the aortic root were affected, the RvD2-GPR18 axis can be assumed to play a role in the progress of the disease rather than in its initiation. In human, atherosclerotic plaques progress from the aortic arch toward the thoracic aorta and are localized in areas with blood flow disturbance (e. g., posterior intercostal arteries) [30]. In this model of short time high fat diet-feeding, we mimicked the development of early plaque development as thoracic aortas plaques were barely detectable.

Taken together the data of the present study suggest that RvD2 protects against atherosclerosis through GPR18 in plaques at a certain stage of immune cell infiltration. Since RvD2 production was preserved in human coronary arteries while GPR18 was dysregulated, the notion of facilitating GPR18 signalling may represent a novel mean to obtain atheroprotection through a functional resolution of inflammation.

Author contribution

MBa, AM, JL, NM, SCP performed experiments and analyzed data. JBM provided human tissue sections and analyzed histology sections. MBa, MBä, SCP, NM, HA, VR, PL, BF designed and supervised the study. MBa, MBä, SCP, JL wrote the manuscript. All authors contributed to the final version of the manuscript.

Acknowledgements

We wish to thank Océane Schlienger for expert technical assistance.

Sources of funding

M Bäck is an awardee of the Gutenberg Chair of Excellence from the Région Grand Est and the Eurométropole de Strasbourg (France). The study was supported by Fondation de France, Lorraine University of Excellence (LUE) Biomolécules, and by grants from the Swedish Research Council (grant number 2019-01486), the Swedish Heart and Lung Foundation (grant numbers 20180571 and 20210560 to M Bäck;

20190625 and 20190196 to H Arnardottir), and the King Gustaf V and Queen Victoria Freemason Foundation. SC Pawelzik was supported by the Professor Nanna Svartz Foundation. M Bardin was supported by a DrEAM (Doctor, Explore, and Achieve More!) mobility grant from the University of Lorraine (grant number R01PKVGX).

References

- [1] M. Bäck, G.K. Hansson, Anti-inflammatory therapies for atherosclerosis, *Nat. Rev. Cardiol.* 12 (4) (2015) 199–211, <https://doi.org/10.1038/nrcardio.2015.5>.
- [2] V.V. Kunjathoor, M. Febbraio, E.A. Podrez, K.J. Moore, L. Andersson, S. Koehn, J. S. Rhee, R. Silverstein, H.F. Hoff, M.W. Freeman, Scavenger receptors class A-I/II and CD36 are the principal receptors responsible for the uptake of modified low density lipoprotein leading to lipid loading in macrophages, *J. Biol. Chem.* 277 (51) (2002) 49982–49988, <https://doi.org/10.1074/jbc.M209649200>.
- [3] E. Thorp, D. Cui, D.M. Schrijvers, G. Kuriakose, I. Tabas, Mertk receptor mutation reduces efferocytosis efficiency and promotes apoptotic cell accumulation and plaque necrosis in atherosclerotic lesions of apoe^{-/-} mice, *Arterioscler. Thromb. Vasc. Biol.* 28 (8) (2008) 1421–1428, <https://doi.org/10.1161/ATVBAHA.108.167197>.
- [4] M. Bäck, A. Yurdagul, I. Tabas, K. Öörni, P.T. Kovanen, Inflammation and its resolution in atherosclerosis: mediators and therapeutic opportunities, *Nat. Rev. Cardiol.* 16 (2019) 389–406, <https://doi.org/10.1038/s41569-019-0169-2>.
- [5] C.N. Serhan, S. Hong, K. Gronert, S.P. Colgan, P.R. Devchand, G. Mirick, R.-L. Moussignac, Resolvins: a family of bioactive products of omega-3 fatty acid transformation circuits initiated by aspirin treatment that counter proinflammation signals, *J. Exp. Med.* 196 (2002) 1025–1037, <https://doi.org/10.1084/jem.20020760>.
- [6] J. Pirault, M. Bäck, Lipoxin and Resolvin Receptors Transducing the Resolution of Inflammation in Cardiovascular Disease, *Front. Pharmacol.* 9 (2018) 1273, <https://doi.org/10.3389/fphar.2018.01273>.
- [7] M.H. Petri, A. Laguna-Fernandez, H. Arnardottir, C.E. Wheelock, M. Perretti, G. K. Hansson, M. Bäck, Aspirin-triggered lipoxin A4 inhibits atherosclerosis progression in apolipoprotein E^{-/-} mice, *Br. J. Pharmacol.* 174 (22) (2017) 4043–4054, <https://doi.org/10.1111/bph.13707>.
- [8] J.R. Viola, P. Lemnitzer, Y. Jansen, G. Csaba, C. Winter, C. Neideck, C. Silvestre-Roig, G. Dittmar, Y. Döring, M. Drechsler, C. Weber, R. Zimmer, N. Cenac, O. Soehnlein, Resolving Lipid Mediators Maresin 1 and Resolvin D2 Prevent Atheroprotection in Mice, *Circ. Res.* 119 (9) (2016) 1030–1038, <https://doi.org/10.1161/CIRCRESAHA.116.309492>.
- [9] H. Hasturk, R. Abdallah, A. Kantarci, D. Nguyen, N. Giordano, J. Hamilton, T. E. Van Dyke, Resolvin E1 (RvE1) attenuates atherosclerotic plaque formation in diet and inflammation-induced atherogenesis, *Arterioscler. Thromb. Vasc. Biol.* 35 (5) (2015) 1123–1133, <https://doi.org/10.1161/ATVBAHA.115.305324>.
- [10] A. Laguna-Fernandez, A. Checa, M. Carracedo, G. Artiach, M.H. Petri, R. Baumgartner, M.J. Forteza, X. Jiang, T. Andonova, M.E. Walker, J. Dalli, H. Arnardottir, A. Gisterå, S. Thul, C.E. Wheelock, G. Paulsson-Berne, D.F. J. Ketelhuth, G.K. Hansson, M. Bäck, ERV1/ChemR23 signaling protects against atherosclerosis by modifying oxidized low-density lipoprotein uptake and phagocytosis in macrophages, *Circulation.* 138 (16) (2018) 1693–1705, <https://doi.org/10.1161/CIRCULATIONAHA.117.032801>.
- [11] H. Arnardottir, S. Thul, S.-C. Pawelzik, G. Karadimou, G. Artiach, A.L. Gallina, V. Mysdotter, M. Carracedo, L. Tarnawski, A.S. Caravaca, R. Baumgartner, D. F. Ketelhuth, P.S. Olofsson, G. Paulsson-Berne, G.K. Hansson, M. Bäck, The resolvin D1 receptor GPR32 transduces inflammation resolution and atheroprotection, *J. Clin. Invest.* 131 (2021), e142883, <https://doi.org/10.1172/JCI142883>.
- [12] M. Drechsler, R. de Jong, J. Rossaint, J.R. Viola, G. Leoni, J.M. Wang, J. Grommes, R. Hinkel, C. Kupatt, C. Weber, Y. Döring, A. Zarbock, O. Soehnlein, Annexin A1 counteracts chemokine-induced arterial myeloid cell recruitment, *Circ. Res.* 116 (5) (2015) 827–835, <https://doi.org/10.1161/CIRCRESAHA.116.305825>.
- [13] E.P.C. van der Vorst, M. Mandl, M. Müller, C. Neideck, Y. Jansen, M. Hristov, S. Gencer, L.J.F. Peters, S. Meiler, M. Feld, A.-L. Geiselhöringer, R.J. de Jong, C. Ohnmacht, H. Noels, O. Soehnlein, M. Drechsler, C. Weber, Y. Döring, Hematopoietic ChemR23 (Chemerin Receptor 23) fuels atherosclerosis by sustaining an M1 macrophage-phenotype and guidance of plasmacytoid dendritic cells to murine lesions—brief report, *Arterioscler. Thromb. Vasc. Biol.* 39 (4) (2019) 685–693, <https://doi.org/10.1161/ATVBAHA.119.312386>.
- [14] G. Fredman, J. Hellmann, J.D. Proto, G. Kuriakose, R.A. Colas, B. Dorweiler, E. S. Connolly, R. Solomon, D.M. Jones, E.J. Heyer, M. Spite, I. Tabas, An imbalance between specialized pro-resolving lipid mediators and pro-inflammatory leukotrienes promotes instability of atherosclerotic plaques, *Nat. Commun.* 7 (2016) 12859, <https://doi.org/10.1038/ncomms12859>.
- [15] M.H. Petri, A. Laguna-Fernández, M. Gonzalez-Diez, G. Paulsson-Berne, G. K. Hansson, M. Bäck, The role of the FPR2/ALX receptor in atherosclerosis development and plaque stability, *Cardiovasc. Res.* 105 (2015) 65–74, <https://doi.org/10.1093/cvr/cvu224>.
- [16] N. Chiang, J. Dalli, R.A. Colas, C.N. Serhan, Identification of resolvin D2 receptor mediating resolution of infections and organ protection, *J. Exp. Med.* 212 (2015) 1203–1217, <https://doi.org/10.1084/jem.20150225>.
- [17] D. McHugh, J. Page, E. Dunn, H.B. Bradshaw, Δ(9)-Tetrahydrocannabinol and N-arachidonyl glycine are full agonists at GPR18 receptors and induce migration in human endometrial HEC-1B cells, *Br. J. Pharmacol.* 165 (2012) 2414–2424, <https://doi.org/10.1111/j.1476-5381.2011.01497.x>.
- [18] M.-A. Mawhin, P. Tilly, G. Zirka, A.-L. Charles, F. Slimani, J.-L. Vonesch, J.-B. Michel, M. Bäck, X. Norel, J.-E. Fabre, Neutrophils recruited by leukotriene B4 induce features of plaque destabilization during endotoxaemia, *Cardiovasc. Res.* 114 (2018) 1656–1666, <https://doi.org/10.1093/cvr/cvy130>.
- [19] S. Thul, C. Labat, M. Temmar, A. Benetos, M. Bäck, Low salivary resolvin D1 to leukotriene B4 ratio predicts carotid intima media thickness: A novel biomarker of non-resolving vascular inflammation, *Eur. J. Prev. Cardiol.* 24 (9) (2017) 903–906.
- [20] A.S. Gandhi, D. Budac, T. Khayrullina, R. Staal, G. Chandrasena, Quantitative analysis of lipids: a higher-throughput LC-MS/MS-based method and its comparison to ELISA, *Future Sci. OA.* 3 (2017) FSO157, <https://doi.org/10.4155/fsoa-2016-0067>.
- [21] S. Koplev, M. Seldin, K. Sukhavasi, R. Ermel, S. Pang, L. Zeng, S. Bankier, A. Di Narzo, H. Cheng, V. Meda, A. Ma, H. Talukdar, A. Cohain, L. Amadori, C. Argmann, S.M. Houten, O. Franzén, G. Mocchi, O.A. Meelu, K. Ishikawa, C. Whatling, A. Jain, R.K. Jain, L.-M. Gan, C. Giannarelli, P. Roussos, K. Hao, H. Schunkert, T. Michoel, A. Ruusalepp, E.E. Schadt, J.C. Kovacic, A.J. Lusis, J.L.M. Björkregren, A mechanistic framework for cardiometabolic and coronary artery diseases, *Nat. Cardiovasc. Res.* 1 (2022) 85–100, <https://doi.org/10.1038/s44161-021-00009-1>.
- [22] D.G. Johns, D.J. Behm, D.J. Walker, Z. Ao, E.M. Shapland, D.A. Daniels, M. Riddick, S. Dowell, P.C. Staton, P. Green, U. Shabon, W. Bao, N. Aiyar, T.-L. Yue, A.J. Brown, A.D. Morrison, S.A. Douglas, The novel endocannabinoid receptor GPR55 is activated by atypical cannabinoids but does not mediate their vasodilator effects, *Br. J. Pharmacol.* 152 (2007) 825–831, <https://doi.org/10.1038/sj.bjp.0707419>.
- [23] G. Artiach, M. Carracedo, J. Clària, A. Laguna-Fernandez, M. Bäck, Opposing Effects on Vascular Smooth Muscle Cell Proliferation and Macrophage-induced Inflammation Reveal a Protective Role for the Proresolving Lipid Mediator Receptor ChemR23 in Intimal Hyperplasia, *Front Pharmacol.* 9 (2018) 1327, <https://doi.org/10.3389/fphar.2018.01327>.
- [24] G. Artiach, M. Carracedo, O. Plunde, C.E. Wheelock, S. Thul, P. Sjövall, A. Franco-Cereceda, A. Laguna-Fernandez, H. Arnardottir, M. Bäck, Omega-3 Polyunsaturated Fatty Acids Decrease Aortic Valve Disease Through the Resolvin E1 and ChemR23 Axis, *Circulation.* 142 (2020) 776–789, <https://doi.org/10.1161/CIRCULATIONAHA.119.041868>.
- [25] A. Lopategi, R. Flores-Costa, B. Rius, C. López-Vicario, J. Alcaraz-Quiles, E. Titos, J. Clària, Frontline Science: Specialized proresolving lipid mediators inhibit the priming and activation of the macrophage NLRP3 inflammasome, *J. Leukoc. Biol.* 105 (2019) 25–36, <https://doi.org/10.1002/JLB.3HI0517-206RR>.
- [26] D.M. Schrijvers, G.R.Y. De Meyer, A.G. Herman, W. Martinet, Phagocytosis in atherosclerosis: Molecular mechanisms and implications for plaque progression and stability, *Cardiovasc. Res.* 73 (2007) 470–480, <https://doi.org/10.1016/j.cardiores.2006.09.005>.
- [27] N. Mercier, M. Bäck, The double-action of hydrogen peroxide on the oxidative atherosclerosis battlefield, *Atherosclerosis.* 331 (2021) 28–30, <https://doi.org/10.1016/j.atherosclerosis.2021.07.001>.
- [28] A. Mahdi, A. Collado, J. Tengbom, T. Jiao, T. Wodaje, N. Johansson, F. Farnebo, A. Färnert, J. Yang, J.O. Lundberg, Z. Zhou, J. Pernow, Erythrocytes Induce Vascular Dysfunction in COVID-19, *JACC Basic Transl. Sci.* (2022), <https://doi.org/10.1016/j.jacbs.2021.12.003>.
- [29] S. Delbos, R.G. Bayles, J. Laschet, V. Ollivier, B. Ho-Tin-Noé, Z. Touat, C. Deschildre, M. Morvan, L. Louedec, L. Gouya, K. Guedj, A. Nicoletti, J.-B. Michel, Erythrocyte Efferocytosis by the Arterial Wall Promotes Oxidation in Early-Stage Atheroma in Humans, *Front. Cardiovasc. Med.* 4 (2017) 43, <https://doi.org/10.3389/fcvm.2017.00043>.
- [30] S. Glagov, D.A. Rowley, R.I. Kohut, Atherosclerosis of human aorta and its coronary and renal arteries. A consideration of some hemodynamic factors which may be related to the marked differences in atherosclerotic involvement of the coronary and renal arteries, *Arch. Pathol.* 72 (1961) 558–571.